Microscopic modeling of transverse non-equilibrium dynamics in mode-locked VECSELs

McLaren, S., Kilen, I., Moloney, J.

S. McLaren, I. Kilen, J. V. Moloney, "Microscopic modeling of transverse non-equilibrium dynamics in mode-locked VECSELs," Proc. SPIE 11263, Vertical External Cavity Surface Emitting Lasers (VECSELs) X, 1126305 (2 March 2020); doi: 10.1117/12.2546310

SPIE.

Event: SPIE LASE, 2020, San Francisco, California, United States

Microscopic modeling of transverse non-equilibrium dynamics in mode-locked VECSELs

S. McLaren[a,b], I. Kilen[b,c], and J. V. Moloney[a,b,c,d]

[a] Program in Applied Mathematics, University of Arizona, 617 N. Santa Rita Ave., Tucson, Arizona 85721, USA

[b] Arizona Center for Mathematical Sciences, 1630 E University Blvd., University of Arizona, Tucson, AZ 85721, USA

[c]Wyant College of Optical Sciences, University of Arizona, 1630 East University Boulevard, Tucson, Arizona 85721, USA

[d] Department of Mathematics, University of Arizona, 617 N. Santa Rita Ave., Tucson, Arizona 85721, USA

ABSTRACT

Mode-locked vertical external-cavity surface emitting lasers are promising compact sources for high-power, ultrafast pulses with excellent beam quality and the flexibility offered by an external cavity. Classical models of these lasers use either phenomenological approaches, which rely heavily on experimentally observed macroscopic parameters, or are based on quasi-equilibrium conditions. Although these models enjoy widespread success, they cannot capture the underlying charge carrier dynamics, shown to be critical components of pulse formation and propagation. The Maxwell Semiconductor Bloch Equations capture these dynamics through a coupling of pulse propagation to the field induced polarization within an active semiconductor quantum well. We utilize a transverse implementation of this model to microscopically investigate fundamental Gaussian pulse formation as well as destabilizing effects of pump parameters. These behaviors are directly linked to the underlying charge carrier dynamics. Excess carriers around the pulse's spatial or spectral centers destabilizes the pulse and are shown to lead to the formation of higher order transverse modes and secondary pulses within the cavity.

Keywords: VECSEL, semiconductor laser, mode-locking, simulation, semiconductor Bloch equations, transverse, instabilities

1. INTRODUCTION

Vertical External Cavity Surface Emitting Lasers (VECSELs) have proven to be highly versatile in producing ultrafast high power pulses with compact and varying geometries.[1–4] These lasers typically are optically pumped, contain of a multilayered semiconductor gain structure, and utilize a semiconductor saturable absorber mirror (SESAM), to achieve mode-locking.[5–8] Under quasi-stationary conditions, where the coherent interband polarization can be adiabatically eliminated, these have had wide-spread success due to their computational ease. However, in the ultrafast dynamic regime, the charge carriers are far from equilibrium and microscopic processes dominate the resulting macroscopic behavior of the system. In order to properly model these processes, one needs to look at the microscopic many-body effects of the gain structure. The Maxwell Semiconductor Bloch Equation (MSBE) model does just that by coupling wave propagation to a polarization source term driven by the underlying semiconductor many-body physics. Herein, we utilize a transverse implementation of this model to study stable, and unstable, mode-locking.

The primary components of the model are the electric field propagation and the field induced polarization which drives pulse formation. In order to compute the polarization response present at a quantum well interface, we note that the macroscopic polarization can be found by integrating over the microscopic polarization states

$$P(t) = \sum_k d_{cv} p_k(t) \tag{1}$$

Further author info:
S. McLaren: E-mail: smclaren@math.arizona.edu

Vertical External Cavity Surface Emitting Lasers (VECSELs) X, edited by Jennifer E. Hastie, Proc. of SPIE Vol. 11263, 1126305 · © 2020 SPIE
CCC code: 0277-786X/20/$21 · doi: 10.1117/12.2546310

wherein d_{cv} is the dipole transition element. We model the microscopic polarization states using the Semiconductor Bloch Equations (SBE).[9] These equations of motion describe the semiconductor response to an incident electric field,

$$\begin{aligned}\frac{\partial}{\partial t}p_k &= -i\omega_k p_k - i\Omega_k(n_k^e + n_k^h - 1) + \Lambda_{spont}^p + \frac{\partial}{\partial t}p_k\Big|_{scatt};\\ \frac{\partial}{\partial t}n_k^{e(h)} &= i\left[\Omega_k p_k^* - \Omega_k^* p_k\right] + \Lambda_{spont}^n + \frac{\partial}{\partial t}n_k^{e(h)}\Big|_{scatt};\end{aligned} \tag{2}$$

Therein, $n_k^{e(h)}$ is the occupation number for electrons (holes) in state k. Our Rabi frequency, Ω_k, and particle energy are renormalized in the Hartree-Fock limit. The renormalized Rabi frequency is given by

$$\Omega_k = \frac{d_{cv}E(z,t)}{\hbar} + \frac{1}{\hbar}\sum_{k\neq q} V_{|k-q|}p_q \tag{3}$$

where $E(z,t)$ is the incident electric field, $\hbar$ is Planck's constant and $V_{|k-q|}$ is the Coulomb potential. The renormalized parabolic two-band single particle energy is given by

$$\hbar\omega_k = \frac{\hbar^2\vec{k}^2}{2m_r} + E_g - \sum_{q\neq k} V_{|k-q|}(n_q^e + n_q^h) \tag{4}$$

where m_r and E_g are the reduced mass and band gap energy, respectively.

Within the SBE, the population inversion, $n_k^e + n_k^h - 1$, governs the amplification of the incident electric field. Where an inversion is positive, an incident field causes carriers to recombine. This reduces carrier populations through the burning of a *kinetic hole*, around the field's spectral, and spatial, centers. This then provides amplification to the pulse. Conversely, for spectral, and spatial, regions of negative inversion, the pulse will see absorption within those regions.

Note that all higher-order particle interactions are contained within our scattering terms. This infinite hierachical system of effects can be modeled at various levels, herein treated up to the Second-Borne Markov approximation. Even at this level, these effects are extremely computationally intensive, making mode-locking simulations impractical. However, it has been shown that under mode-locking conditions scattering can be well approximated by appropriate exponential decay and recovery.[10] The polarization dephasing is modeled using a single decay rate

$$\frac{\partial}{\partial t}p_k\Big|_{scatt} = -\frac{1}{\tau_{deph}}p_k. \tag{5}$$

The occupation number scattering terms are modeled using a dual rate recovery,

$$\frac{\partial}{\partial t}n_k^{e(h)}\Big|_{scatt} = -\frac{1}{\tau_{scatt}}\left(n_k^{e(h)} - f_k^{e(h)}\right) - \frac{1}{\tau_{fill}}\left(n_k^{e(h)} - F_k^{e(h)}\right). \tag{6}$$

On a fast time scale, τ_{fill}, the carriers recover to an instantaneous Fermi distribution, $F_k^{e(h)}$, based on current temperatures and densities. This kinetic hole filling is driven by carrier scattering. On a much slower scale, τ_{scatt}, the carriers recover to the static background Fermi distribution of the pump, $f_k^{e(h)}$.

Spontaneous emission is modeled phenomenologically with $\Lambda_{spont}^n = -\Lambda_k^{spont}n_k^e n_k^h$ and $\Lambda_{spont}^p = \beta\Lambda_k^{spont}n_k^e n_k^h$.[11] Therein, β is a randomly distributed phase and

$$\Lambda_k^{spont} = \frac{n_{bgr}^3}{\pi^2\epsilon\hbar^4c_0^3}|d_{cv}|^2\left(\frac{\hbar^2\vec{k}^2}{2m_r} + E_g\right)^3. \tag{7}$$

The propagation of the electric field within the cavity is modeled using Maxwell's wave equation

$$\left[\frac{\partial^2}{\partial z^2} - \frac{n_b^2}{c_0^2}\frac{\partial^2}{\partial t^2}\right]E(z,t) = \mu_0\frac{\partial^2}{\partial t^2}P(z,t). \tag{8}$$

wherein n_b, c_0, and μ_0 are the material refractive index, vacuum speed of light, and vacuum permittivity, respectively.

The cavity is oriented linearly and consists of a gain structure and saturable absorber, separated by a large air gap. The modeled gain structure consists of a single effective QW optimally placed to recreate the result obtained from a one-dimensional simulation of a resonant periodic gain (RPG) structure of 10 $8nm$ AlGaAs quantum wells. This QW is backed by a 61 layer distributed Bragg reflector (DBR) consisting of alternating layers of AlGaAs and AlAs, and is coated with a bilayer antireflective (AR) coating composed of Ta_2O_5 and SiO_2 and an InGaP cap layer. The SESAM, a single unpumped QW, is coated with Si_3N_4, and has a 1% loss out the back to introduce an output coupling (OC) loss. The dephasing and kinetic hole filling rates were taken as $\tau_{deph} = 47fs, \tau_{fill} = 100fs$. The slow scattering of the gain chip and rapid scattering of the absorber, $\tau_{scat,g(a)}$ were taken as $\tau_{scat,g} = 30ps$ and $\tau_{scat,a} = 2ps$ respectively. Between these elements are two air cavities, $L_1 = 49.054mm$, $L_2 = 6.622mm$, separated by a lens, $f = 6.1936mm$, chosen for a desired spot size ratio between the gain chip and SESAM. The wave propagation is numerically integrated using a pseudospectral solver for the air regions, linear transport for the inactive semiconductor structures and a phase mask for the lens. Due to this judicious choice of numerical solvers, diffraction and propagation time are decoupled, so that the round-trip time can be taken independently of the true propagation distance. In general, the cavity length delays the pulse interaction with the QWs and is chosen appropriately to produce a desired stable mode-locked pulse. The SBE are integrated using a fourth-order Runge-Kutta method. To hasten the convergence of the simulation, a low energy seed pulse is used within the cavity. A natural first goal is to achieve stable fundamental mode-locking as a baseline for future research.

2. FUNDAMENTAL OPERATION

Stable fundamental transverse mode operation requires careful attention to the setup of the cavity. Particularly, the transverse pump profile needs to be tuned to not provide excess carriers along the spectral or transverse wings of the pulse. Shown in Fig. 1 is the initial Super-Gaussian pump profile with a $336\mu m$ spot size and a peak total carrier density of $n_0 = 2.35E16m^{-2}$. This corresponds to a pulse to pump spot size ratio of $w_0/w_p = 0.6$. The associated temperature profile was obtained numerically through a COMSOL multiphysics simulation from previous work.[12]

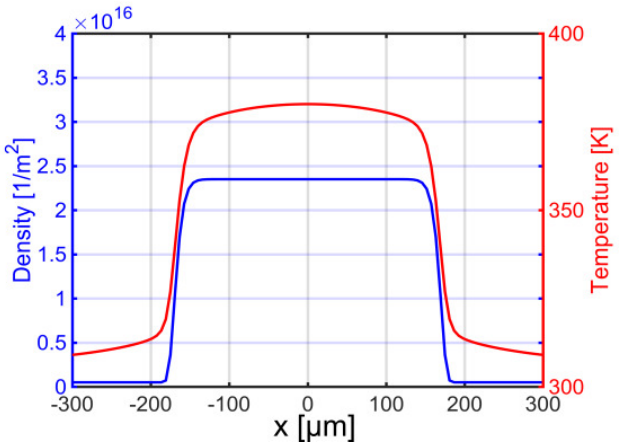

Figure 1. Initial Super-Gaussian pump density profile and numerically obtained temperature profile. Pump has a peak density of $n_0 = 2.35E16m^{-2}$ and a spot size of $336\mu m$ spot size and corresponds to a pulse to pump spot size ratio of $w_0/w_p = 0.6$.

Shown in Fig. 2 is the evolution of the temporal and spatial full width half maximums (FWHM) for the given simulation. Within $60ns$, the pulse converges to temporal and spatial FWHM of $89.4fs$ and $147\mu m$, respectively. This illustrates that the simulation has converged.

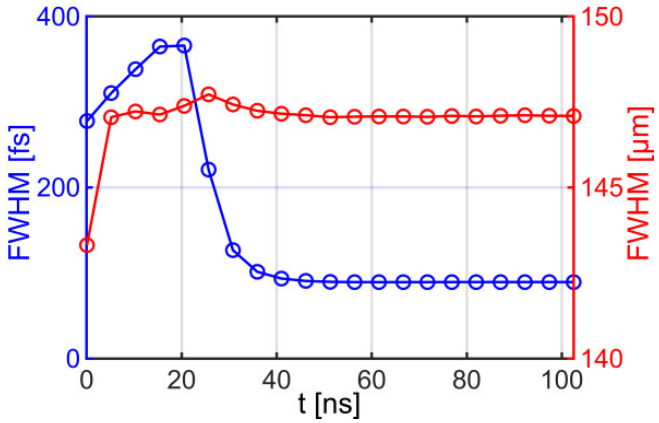

Figure 2. Fundamental mode operation simulation convergence of the temporal and spatial FWHM using a pulse to pump spot size ratio of $w_0/w_p = 0.6$ and a peak density of $n_0 = 2.35E16m^{-2}$.

To conclusively show that the simulation has converged to fundamental mode operation, shown in Fig. 3 is the growth of the transverse intensity profile at the peak of the pulse overlaid with the pump distribution in black. The stabilized transverse Gaussian profile can clearly be seen. This, along with the stabilized FWHM, demonstrates convergence to a stable fundamental transverse mode pulse.

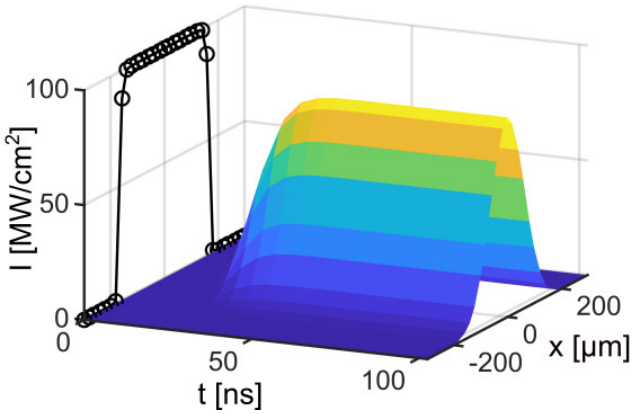

Figure 3. Evolution of the transverse intensity profile at the peak of the pulse using a pulse to pump spot size ratio of $w_0/w_p = 0.6$ and a peak density of $n_0 = 2.35E16m^{-2}$.

Shown in Video 1 are the population inversion dynamics across the entire pump distribution. As the pulse enters the pumped QW, carriers recombine and a kinetic hole burns around the pulse's spectral and spatial centers. As the pulse leaves the QW, the kinetic hole recovers towards the background pumping distribution. While the pulse is weak, carriers are not deformed far from Fermi distributions. As the pulse grows, so does the kinetic hole, reducing the available carriers in this region. Over thousands of round-trips, the growth and recovery stabilizes into a single fundamental transverse mode pulse.

In the stable case, the pulse burns a single kinetic hole in the population inversion. The availability of excess carriers along the spatial and spectral wings of the pulse leads to the burning of distinct kinetic holes and, ultimately, pulse destabilization.

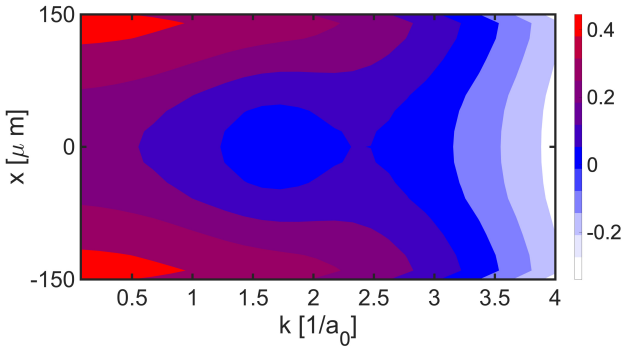

Video 1. Kinetic hole burning within the population inversion for simulation shown in Figs. 2 and 3. http://dx.doi.org/10.1117/12.2546310.1

3. UNSTABLE OPERATION

In order to improve VECSELs, it is critical to understand their mechanisms of destabilization. Fundamentally, positive inversions promote pulse amplification and negative inversions lead to pulse absorption. To sustain pulse growth on successive round-trips, the inversion must be large enough to produce a net gain within the cavity. As the intensity of the pulse increases, the kinetic hole it burns deepens. If the inversion remains large along the spatial or spectral wings of the pulse, then the pulse will be amplified along these wings, leading to the generation of higher order transverse modes and secondary pulses.

Shown in Fig. 4 is a late output after $t = 598ns$ of simulation time for an unstable simulation using a low pulse to pump spot size ratio, $w_0/w_p = 0.3$, and a high peak total carrier density of $n_0 = 3.0E16m^{-2}$. Within a single round-trip, six separate pulses are present within the cavity. Fig. 4(a) shows the transverse profiles at the peaks of these pulses. The number, position, and relative size of the peaks within these pulses varies. However, looking at the integrated transverse intensity of these pulses, as shown in Fig. 4(b), we see that the temporal profile of these pulses is closely Gaussian in nature. Thus, poor beam quality could easily be masked by merely looking at integrated power outputs.

A natural first step to try to explain this behavior is to look at the total carrier density evolution. The dynamics of this macroscopic parameter is shown in Fig. 5 for a single round-trip. One can see each of the six pulses hitting the QW, indicated by a drop in total carrier density. However, the shape of the incident pulse cannot readily be deduced from this. This is because total carrier density is a derived macroscopic quantity which integrates out critical spectral data.

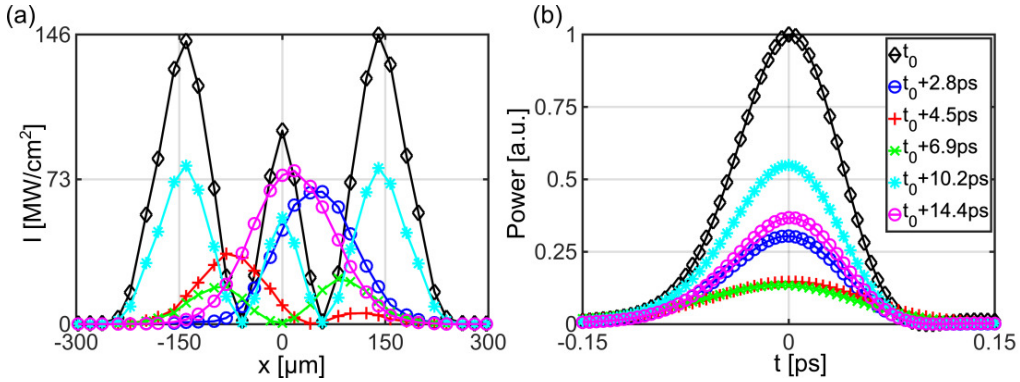

Figure 4. (a) Transverse profiles at peak of pulses, and (b) integrated transverse intensity as measure of pulse powers, for unstable multipulsing operation with higher order transverse modes for a wide pump, $w_0/w_p = 0.3$ with a high peak carrier density, $n_0 = 3.0E16m^{-2}$ over a single round-trip.

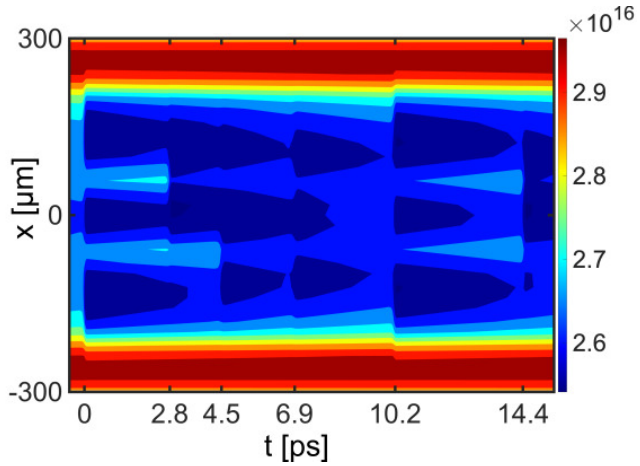

Figure 5. Total carrier density evolution over a single round-trip for unstable multipulsing operation with higher order transverse modes for a wide pump, $w_0/w_p = 0.3$ with a high peak carrier density, $n_0 = 3.0E16m^{-2}$ over a single round-trip.

Video 2 shows the population inversion evolution within the gain chip QW, the driver behind the macroscopic behaviors. The video shows the burning of kinetic holes as various pulses enter the QW. The excess of carriers along both the transverse and spectral axes, implies that these holes can be burned freely in either direction. The kinetic hole depths continue to grow on successive round-trips until they are balanced by the amount of total loss within the system. This is not a necessarily stable state, as energy can still move temporally or transversally within the cavity without any change in total cavity energy.

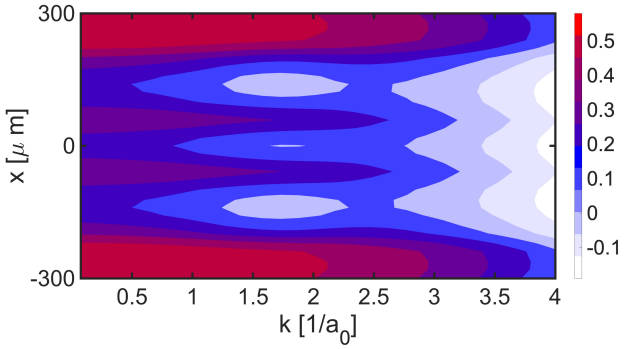

Video 2. Kinetic hole burning within the population inversion for simulation shown in Figs. 4 and 5. http://dx.doi.org/10.1117/12.2546310.2

Once a cavity destabilizes, it is unlikely to restabilize without a reduction in pump intensity or width. Kinetic hole burning, pitted against restrictive cavity modes, gives rise to endless carrier chasing as energy moves between various cavity modes.

4. CONCLUSION

Pulse formation and destabilization within VECSELs was demonstrated and explained through the driving microscopic many-body effects. The presence of carriers within a QW, with an incident pulse, gives rise to kinetic hole burning about the pulse's spatial and spectral centers. This significantly deforms carriers away from Fermi distributions. Once the pulse leaves, carriers recover towards their initial excited states. Kinetic hole burning along the spatial and spectral wings of a pulse leads to undesirable amplification at these locations. This ultimately causes the generation of higher order transverse modes and secondary pulses. It was shown that

a narrow pulse to pump spot size ratio, $w_0/w_p = 0.6$ with a low total carrier density, $2.35E16m^{-2}$ is capable of leading to fundamental mode operation. By widening the spot size ratio, $w_0/w_p = 0.3$ and increasing the total carrier density, $n_0 = 3.0E16m^{-2}$ excess carriers destabilize the pulse. Thus, careful control of pump width and intensity, coupled with diagnostic tools that go beyond integrated power outputs, are crucial for the proper stabilization, and characterization, of VECSELs.

ACKNOWLEDGMENTS

This material is based upon work supported by the Air Force Office of Scientific Research under Grant No. FA9550-17-1-0246 and the National Defense Science & Engineering Graduate Fellowship (NDSEG) Program.

REFERENCES

[1] Rahimi-Iman, A., "Recent advances in vecsels," *Journal of Optics* **18** (2016).

[2] Tropper, A. C., Foreman, H. D., Granache, A., Wilcox, K. G., and Hoogland, S. H., "Vertical-external-cavity semiconductor lasers," *Journal of Physics D: Applied Physics* **37**, 75–85 (April 2004).

[3] Tropper, A. C., Quarterman, A. H., and Wilcox, K. G., "Ultrafast Vertical-External-Cavity Surface-Emitting Lasers," in [*Advances in Semiconductor Lasers*], Coleman, J. J., Bryce, A. C., and Jagadish, C., eds., **86**, ch. 7, Elsevier Inc. (2012).

[4] Tilma, B. W., Mangold, M., Zaugg, C. A., Link, S. M., Waldburger, D., Klenner, A., Mayer, A. S., Gini, E., Golling, M., and Keller, U., "Recent advances in ultrafast semiconductor disk lasers," *Light: Science & Applications* **4** (July 2015).

[5] Haus, H. A., "Mode-locking of lasers," *IEEE Journal on Selected Topics in Quantum Electronics* **6**, 1173–1185 (November 2000).

[6] Gurevich, S. V. and Javaloyes, J., "Spatial instabilities of light bullets in passively-mode-locked lasers," *Physical Review A* **96**(023821) (2017).

[7] Hausen, J., Meinecke, S., Lingnau, B., and Lüdge1, K., "Pulse cluster dynamics in passively mode-locked semiconductor vertical-external-cavity surface-emitting lasers," *Physical Review Applied* **11**(044055) (2019).

[8] Mulet, J. and Balle, S., "Mode-locking dynamics in electrically driven vertical-external-cavity surface-emitting lasers," *IEEE Journal of Quantum Electronics* **41**(9) (2005).

[9] Haug, H. and Koch, S. W., [*Quantum Theory of the Optical and Electronic Properties of Semiconductors*], World Scientific, 4 ed. (2004).

[10] Hader, J., Scheller, M., Laurain, A., Kilen, I., Baker, C., Moloney, J. V., and Koch, S. W., "Ultrafast non-equilibrium carrier dynamics in semiconductor laser mode-locking," *Semiconductor Science and Technology* **32** (November 2017).

[11] Bäumner, A., Koch, S. W., and Moloney, J. V., "Non-equilibrium analysis of the two-color operation in semiconductor quantum-well lasers," *Physica Status Solidi B* **248**, 843–846 (September 2011).

[12] Laurain, A., Hader, J., and Moloney, J. V., "Modeling and optimization of transverse modes in vertical-external-cavity surface-emitting lasers," *Journal of the Optical Society of America B* **36** (April 2019).